



# Dynamic Electrical-Mechanical Energy Coupling in Electrolyte-Mineral Systems

*(Low Frequency Range)*

J. CARLOS SANTAMARINA<sup>1</sup> and DANTE O. FRATTA<sup>2</sup>

<sup>1</sup>*Department of Civil and Environmental Engineering, Georgia Tech, 305 Fest Drive, GA 30332-0363, U.S.A.*

<sup>2</sup>*Louisiana State University, Baton Rouge, LA 70803, U.S.A.*

(Received: 22 November 2000; in final form: 12 December 2001)

**Abstract.** Electrical-mechanical and mechanical-electrical coupling phenomena have been observed in geo-materials. Underlying internal phenomena are not always clear. In this paper, we identify potential microscale processes on the bases of previously published research; fundamental physical principles and analytical models are included. Second, we notice important inconsistencies between theoretically predicted values or high-frequency laboratory data with respect to low-frequency field observations. To explore these differences, we conduct a laboratory experimental study that simulates field conditions, placing emphasis on low frequency coupling, that is, less than 10 kHz. Both, mechanical-electrical and electrical-mechanical effects are observed. Finally, hypotheses are presented in an attempt to explain observed differences.

**Key words:** energy coupling, electrical-mechanical coupling, mechanical-electrical coupling, soils, particulate media, electrolyte, diffuse double layer, electromagnetic waves, mechanical waves, electro-seismic effects, seismo-electric effects, laboratory measurements, electrode polarization.

## 1. Introduction

Electrical-mechanical and mechanical-electrical coupling phenomena are supported by fundamental physical principles including energy conservation, energy coupling, and Le Châtelier's principle (the effects are labeled as 'cause-effect'). The principle of energy conservation postulates that energy can be transformed from one form to another, and transferred from one body to another, but the total amount of energy in the system remains constant. Energy coupling refers to the inherent link between energy in its different forms, that is, thermal, mechanical, chemical, and electrical. Le Châtelier's principle states that a system in equilibrium will oppose any disturbance; for example, enforcing a thermal gradient in a medium causes counter chemical, electrical, and mechanical gradients. Common examples of energy coupling include: thermal expansion which relates mechanical and thermal energies, piezoelectricity which links mechanical and electrical energies, and pyroelectricity which relates electrical and thermal energies (Holden, 1965; Ikeda, 1990; Mitchell, 1991). In the case of granular and porous media, the coupling between mechanical and electrical energy has different manifestations, known as electro-kinetic phenomena (Lyklema, 1995).

Table I. Examples of mechanical-electrical and electrical-mechanical energy coupling

Input	Output			
	Mechanical	Electro-magnetic	Chemical	Thermal
Mechanical	<ul style="list-style-type: none"> <li>• Stimulated AE</li> <li>• Stress-strain</li> </ul>	<ul style="list-style-type: none"> <li>• Piezo-electricity</li> <li>• Photo-elasticity</li> <li>• Seismo-electricity</li> </ul>	<ul style="list-style-type: none"> <li>• Phase transform.</li> <li>• Stimulated reactions</li> </ul>	<ul style="list-style-type: none"> <li>• Frictional heating</li> <li>• Thermo-elasticity</li> </ul>
Electro-magnetic	<ul style="list-style-type: none"> <li>• AE (differential thermal expansion)</li> <li>• Electro-seismicity</li> <li>• Magneto-strictive</li> <li>• Fracture control with magnetic field</li> </ul>	<ul style="list-style-type: none"> <li>• Absorption and infrared radiation</li> <li>• Laser</li> <li>• Fluorescence</li> </ul>	<ul style="list-style-type: none"> <li>• Phase transform.</li> <li>• Stimulated reactions</li> <li>• Photosynthesis</li> </ul>	<ul style="list-style-type: none"> <li>• Electromagnetic heating<sup>a</sup></li> </ul>
Chemical	<ul style="list-style-type: none"> <li>• AE (due to phase transformation reactions)</li> <li>• Explosions</li> </ul>	<ul style="list-style-type: none"> <li>• Chemico-luminescence</li> <li>• Bio-luminescence</li> <li>• Electro-chemistry</li> </ul>	<ul style="list-style-type: none"> <li>• Secondary reactions</li> </ul>	<ul style="list-style-type: none"> <li>• Thermo-chemistry</li> <li>• Metabolism</li> <li>• Combustion–oxidation</li> </ul>
Thermal	<ul style="list-style-type: none"> <li>• AE (differential thermal expansion)</li> <li>• Thermal fracture (e.g. spalling)</li> </ul>	<ul style="list-style-type: none"> <li>• Thermo-luminescence</li> <li>• Pyro-electricity</li> </ul>	<ul style="list-style-type: none"> <li>• Thermo-chemistry</li> <li>• Photosynthesis</li> <li>• Phase transform.</li> <li>• Stimulated reactions</li> </ul>	<ul style="list-style-type: none"> <li>• Thermal response (heat transfer)</li> </ul>

<sup>a</sup>Underlying phenomena depend on frequency.

Energy coupling develops not only under steady state condition, but in dynamic events as well, including wave propagation phenomena. Table I presents some known examples of direct and indirect dynamic coupling phenomena in wave propagation. While continuity and equilibrium preserve frequency content (e.g. wave propagation across boundaries), careful analysis of causal processes can justify different frequencies in coupled wave phenomena.

Dynamic energy coupling in geo-materials has been studied for more than 60 years with different degrees of success. Thompson (1936) notes that the resistivity of the ground changes when it is subjected to elastic deformation. Bellugi (1937) discusses possible uses of this effect and suggests a circuit to develop an 'electro-elastic seismometer.' Later, Martner and Sparks (1958) report the generation of an electric potential in the ground during the passage of seismic waves while monitoring explosions from boreholes with surface electrodes. More recently, observations of mechanical-electrical coupling have been made during near-surface seismic prospecting. The relative timing of events points to generation mechanisms located in the partially saturated and saturated portions of the deposit, and at boundaries between different strata. In spite of these measurements, there is no systematic field or laboratory study of electromagnetic-mechanical dynamic coupling in soils. Analytical efforts to model electrical-mechanical and mechanical-electrical coupling phenomena starts with the work on electrolytes by Debye in the 1930s, and on poroelastic media by Frenkel in the 1940s.

This paper starts with a fundamental description of soils and a review of the unique aspects of elastic and electromagnetic wave propagation in particulate media, in view of the subsequent discussion of mechanical-electrical couplings. Afterwards, the results from this research are organized into four main parts. First, micro-scale mechanisms that explain dynamic mechanical-electrical energy coupling in electrolytes, suspension, and soils are identified on the bases of published results. Second, theoretically predicted values, laboratory measurements, and field measurements are tabulated and compared. Third, a unique device is designed to measure electrical-mechanical and mechanical-electrical coupling in soil specimens to simulate field conditions, and experimental results are presented for electrolytes and soils in the frequency range relevant to field applications. Finally, various hypotheses are presented to explain differences between the response measured in the field and theoretical or standard laboratory results.

## 2. Soils and Waves

Soils involve mineral grains forming a porous skeleton. The transmission of skeletal forces and the movement of grains are not homogeneous within the skeleton. In fact, aggregations of grains can often be identified. So there are at least two internal scales: grain size and aggregation size. The interconnected pores are filled with fluid, for example, air, water, organics, or a mixture. Within the context of this study, the pore fluid is an aqueous electrolyte.

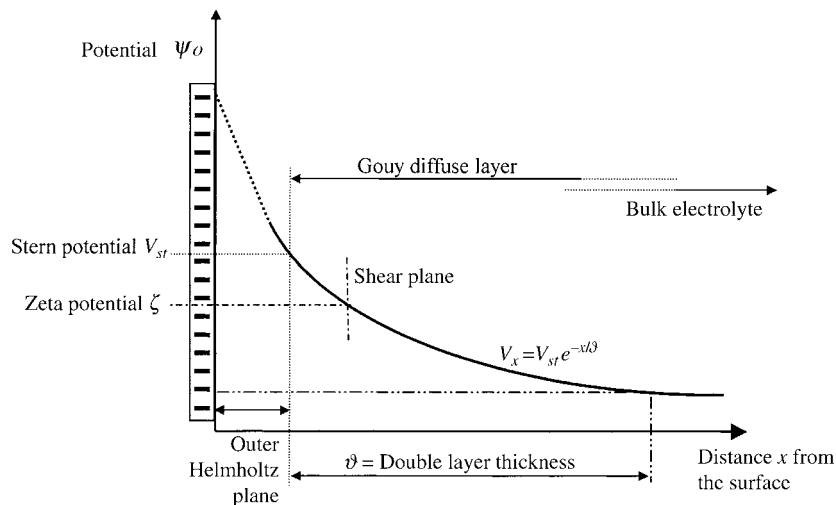


Figure 1. Double layer at a mineral-electrolyte interface. The double layer thickness  $\vartheta$  is the distance where the potential drops to  $V_{st}/e$ . Ions outside the shear plane move with the bulk electrolyte.

Under normal pH conditions, the mineral surface exhibits negative surface charge. Therefore, hydrated cations are attracted and hydrated anions are repelled. The balance between electrical forces among charges and thermal agitation renders a particular charge distribution in the vicinity of particles, known as the double layer (Figure 1). When the pore fluid moves relative to the particle, part of the ionic cloud moves with the fluid; for simplicity, a sharp shear plane is often assumed. The potential on the shear plane is the zeta-potential.

From a mechanical point of view, soils are two-phase poroelastic media. While there are only two modes of wave propagation in a single-phase isotropic continuum, that is, P and S-waves, a third mode develops in a poroelastic medium: the diffusional slow-P wave. The hydraulic conductivity of the formation and the relative mass densities of the solid matrix and the fluid phase govern the behavior of the slow P-wave (Stoll, 1977; White, 1983; Bourbié *et al.*, 1987). A repetitive discrete medium acts as a low-pass filter for the propagation of elastic waves; that is, only waves with wavelength much larger than the internal scale of the medium are transmitted. For most engineering and field applications, stress wave propagation is restricted to frequencies below 10 kHz.

From an electrical point of view, a soil mass is equally elaborate. The grains are most often made of low-conductivity and low-permittivity minerals (conductivity  $\sigma = 10^{-15}$  S/m, and relative permittivity  $\kappa' = 4.2-5.0$ ). The electrolyte filling the voids has high permittivity (e.g. the relative permittivity of water is  $\kappa' = 80$ ) and its conductivity is directly proportional to the ionic concentration (linear relation at low concentrations). Double layers around minerals contribute surface conduction to the global conductivity of the soil mass. The relevance of surface conduction to global conduction is proportional to the specific surface of the soil and vanishes

as the conductivity of the electrolyte increases. Therefore, surface conduction is most important in fine-grained soils saturated with low ionic concentration fluids. When the mixture is subjected to an oscillating electric field in the radio frequencies ( $f < 1$  MHz), hydrated ions in the double layer and in the pore fluid move in the direction of the field. However, the presence of particle surfaces normal to the direction of the field blocks the movement of ions, resulting in interfacial Maxwell–Wagner polarization. Overall, as the frequency decreases the permittivity of the medium increases and the effective AC conductivity decreases.

### 3. Identification of Coupling Mechanisms in Electrolytes

The next two sections center on the identification of mechanical-electrical and the electrical-mechanical dynamic coupling mechanisms, on the bases of prior studies and published evidence. This section addresses electrolytes. The effect of mineral particles is considered in the context of suspensions and soils in the next section.

#### 3.1. MECHANICAL-ELECTRICAL COUPLING

Consider the electrically neutral system shown in Figure 2(a). The difference in inertia between positive and negative charges causes their relative displacement when subjected to a mechanical excitation, resulting in an electrical current. Each charged element is of radius  $r$  [m] and mass  $m$  [kg], has a charge of  $z$  electron charges  $e_o = 1.6 \times 10^{-19}$  C, and moves at velocity  $v$  [m/s]. There are  $n$  such charged elements per liter of solution. The position  $x$  of charged components in a mass is constrained by three laws: equilibrium, continuity, and Poisson's equation. At any given time  $t$ , these three laws are (in these equations, the subscripts '+' and '-' refer to the positive or the negative charged elements and the subscript 's' to the rest of the mass):

$$(e_o z_+)E = m_+ \frac{\partial v_+}{\partial t} + \psi_+(v_+ - v_o) \quad \text{equilibrium,} \quad (1)$$

$$\frac{\partial n_+}{\partial t} + \frac{\partial}{\partial x}(n_+ v_+) = 0 \quad \text{conservation of charge,} \quad (2)$$

$$\frac{\partial E}{\partial x} = \frac{4\pi e_o}{\kappa \epsilon_o}(n_+ z_+ + n_- z_-) \quad \text{poisson's equation,} \quad (3)$$

where  $v_o$  is the velocity of the medium [m/s]. Similar equations of equilibrium and charge conservation are written for the negative charges. The other parameters are the electrical permittivity of free space  $\epsilon_o = 8.85 \times 10^{-12}$  F/m, and the relative permittivity of the medium  $\kappa$  [ ]. The equilibrium equation equates the electrical force generated by the electric field  $E$  to the sum of the inertial force and the viscous

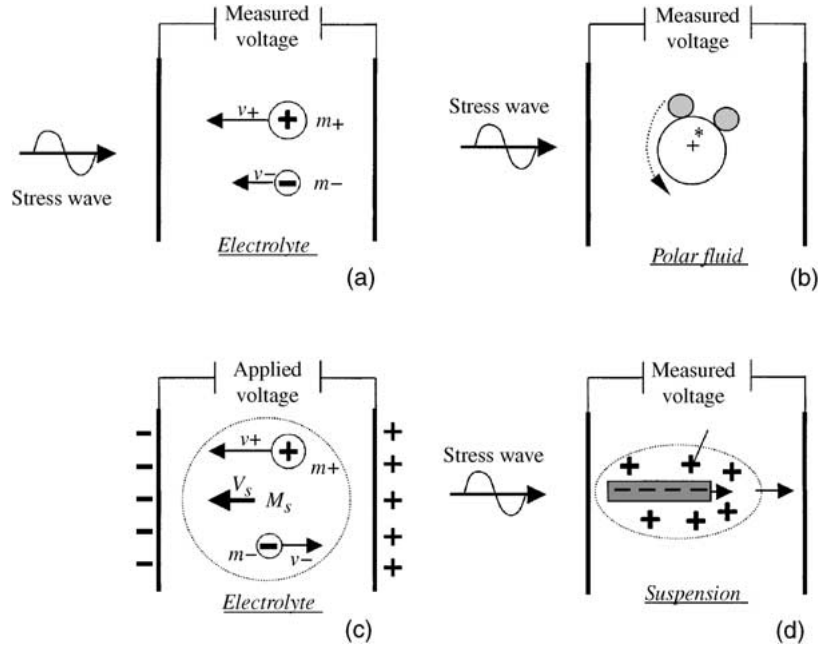


Figure 2. Dynamic energy coupling phenomena. (a) Mechanical-electrical coupling in electrolytes. (b) Mechanical-electrical coupling in polar fluids; a water molecule is sketched, where '+' is center of gravity and '\*' is the center of rotation. (c) Electrical-mechanical coupling in electrolytes. (d) Mechanical-electrical coupling in suspensions. Electrodes are shown in bold lines.

force. The viscous force depends on the relative velocity between the charge and the fluid, and the viscosity factor  $\Psi$  [N·s/m]

$$\psi = 6\pi \cdot \eta \cdot r, \quad (4)$$

where  $\eta$  [Pa·s] is the viscosity of the solvent. (Note: The equilibrium equation for poroelastic media will include other forces related to the stiffness of the system.) The solution for the resulting electric potential  $\phi$  [V] is obtained by assuming a harmonic fluctuation for the electric field and charge motions, leading to the following expression (Debye, 1933; Zana and Yeager, 1982):

$$\begin{aligned} \phi(t) = & \frac{m_H}{e_o} v_o V \frac{(z_- m_-^{\text{ap}}/r_-) - (z_+ m_+^{\text{ap}}/r_+)}{(z_-^2/r_-) + (z_+^2/r_+)} \times \\ & \times \frac{4\pi(\sigma/\kappa\epsilon_o\omega)}{\sqrt{1 + (4\pi(\sigma/\kappa\epsilon_o\omega))^2}} e^{j(\omega t - \kappa x - \Delta)} \quad \text{Debye's equation,} \end{aligned} \quad (5)$$

where  $m_H = 1.66 \times 10^{-27}$  kg is the mass of the hydrogen atom,  $m_+^{\text{ap}}$  and  $m_-^{\text{ap}}$  [ ] are the apparent molecular masses of the positive and negative ions,  $V$  is the P-wave velocity in the medium [m/s],  $\sigma$  is the conductivity of the medium [S/m],  $\omega$  is the angular frequency [ $\text{s}^{-1}$ ],  $\kappa = 2\pi/\lambda$  is the wave number [ $\text{m}^{-1}$ ],  $\lambda$  is the wavelength

of the elastic wave in the solution [m],  $\Delta = \tan^{-1}[\omega\epsilon/(4\pi\sigma)]$  is the phase angle between the elastic wave and the voltage response, and  $j^2 = -1$  is the imaginary number. The phase shift is very small for frequencies below 100 kHz.

The factor  $v_o V$  may be substituted by various relations to help data interpretation. In particular,  $v_o V$  is equal to the ratio between the stress amplitude of the propagating wave and the mass density of the medium. Furthermore, the ratio  $z/r$  can be expressed in terms of the ionic mobility  $u$ , which is the velocity the charged element attains in an electric field. Equating the electrical force to the viscous drag, the ionic mobility  $u$  [ $\text{m}^2/\text{s/V}$ ] is

$$u \equiv \frac{v_+ - v_o}{E} = \frac{z}{r} \frac{e_o}{6\pi\eta} = z \frac{e_o}{\psi} = z \frac{e_o}{kT} D \quad \text{Einstein-Nernst relation,} \quad (6)$$

where  $k = 1.381 \times 10^{-23}$  J/°K is Boltzmann's constant,  $T$  [°K] is temperature, and  $D$  [ $\text{m}^2/\text{s}$ ] is the diffusion coefficient.

The amplitude of the potential  $\phi_o$  predicted by Equation (5) (factors in front of the exponential term) is the maximum potential difference that is measured at a point with respect to the time-averaged potential. As the longitudinal elastic wave propagates, charge accumulates with a periodicity of a wavelength  $\lambda$  as shown in Figure 3. Then, the maximum potential difference that can be measured occurs when the two electrodes are at a distance  $\lambda/2$  apart and it is equal to  $2\phi_o$ .

The phenomenon and the fundamental formulation shown above apply to electrolytes, where the 'charged elements' are hydrated ions (Debye, 1933). In this case, the charge is the ion valence times  $e_o = 1.6 \times 10^{-19}$  C, the size  $r$  is the hydrated radius (e.g. Na:  $r_+ = 0.358$  nm; Cl:  $r_- = 0.332$  nm), and the mass  $m$  involves the mass of the ions plus the mass of hydrating water molecules (e.g. Na: 4–5 water molecules; Cl: about 1 water molecule – Israelachvili, 1992; Santamarina *et al.*, 2001). Figure 4 presents the electrical response predicted with Debye's equation (5) for four different electrolytes. While the mechanical-electrical potential increases with concentration, experimental results show that the effect of concentration vanishes as  $c \rightarrow 10^{-3}$  molar (Zana and Yeager, 1982). Several modifications have

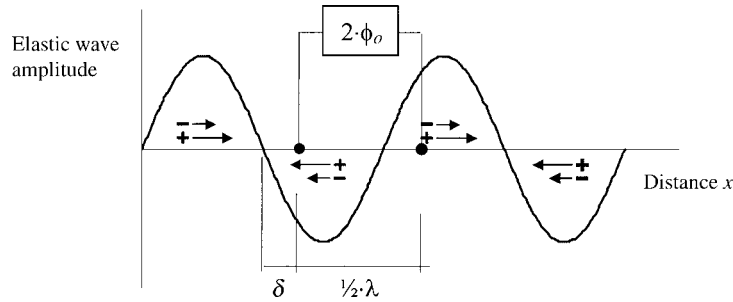


Figure 3. Mechanical-electrical coupling. The maximum potential is measured with electrodes placed  $\lambda/2$  apart, and it is equal to  $2\phi_o$  where  $\phi_o$  is the amplitude of the potential predicted by the Debye's equation. The phase shift  $\delta$  between the elastic wave and the potential is generally very small below 100 kHz.

## Model Parameters

<i>Na ion:</i>		<i>Ca ion:</i>	
Hydrated radius	$r = 0.358 \text{ nm}$	Hydrated radius	$r = 0.412 \text{ nm}$
Hydration number	$N_h = 5 \pm 1$	Hydration number	$N_h = 6 \pm 1$
Valence	$z = +1$	Valence	$z = +2$
<i>K ion:</i>		<i>Cl ion:</i>	
Hydrated radius	$r = 0.332 \text{ nm}$	Hydrated radius	$r = 0.332 \text{ nm}$
Hydration number	$N_h = 4 \pm 2$	Hydration number	$N_h = 1 \pm 1$
Valence	$z = +1$	Valence	$z = -1$

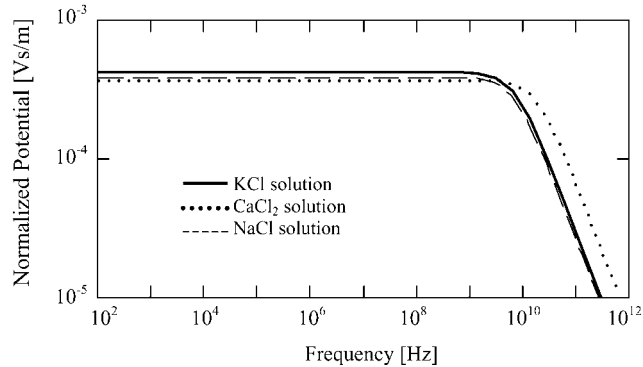


Figure 4. Normalized mechanical-electrical response in 0.5M electrolytes predicted by Debye's (1933) model. Model parameters are summarized in the table (the hydration number is the number of water molecules bound per ion).

been proposed to include other forces in the equilibrium equation. (Hermans, 1938; Zana and Yeager, 1982, include relaxation, electro-phoretic; diffusion and pressure gradient forces).

The rotational motion of dipolar molecules can also generate a mechano-electrical response. Rotation takes place if the center of rotation in the dipolar molecule does not coincide with the center of gravity. As molecules rotate, individual dipole moments align causing an electric field (Figure 2(b)). Thermal excitation and the interaction between neighboring molecules oppose alignment and weakens this coupling effect. This phenomenon is a special case of ultrasonic vibration potential (Lyklema, 1995).

### 3.2. ELECTRICAL-MECHANICAL COUPLING

When the electrical-mechanical coupling is seen from an external frame of reference, it manifests a distinct difference with the mechanical-electrical coupling: the applied electric field makes charges of opposite sign move in opposite directions (Figure 2(c)). The viscous drag transmitted to the fluid causes the motion of the whole mass  $M_s$ . Besides the equation of equilibrium (Equation (1)), the conservation of momentum equation is invoked in this analysis. Assuming that the system



remains electrically neutral, the total impulse applied by the electric field onto the charges is zero, that is,  $q^+ E dt + q^- E dt = 0$ . Then,

$$0 = M_s dv_o + (n_+ m_+) dv_+ + (n_- m_-) dv_- \quad \text{conservation of momentum. (7)}$$

Invoking equilibrium equations and the conservation of momentum, an expression is obtained for the velocity the mass will experience due to the excitation of the internal charged elements

$$v_o = \frac{E \cdot e_o (z_+ m_+ / r_+) n_+ - (z_- m_- / r_-) n_-}{6\pi \cdot \eta (M_s - (n_+ m_+ - n_- m_-))} \quad \text{low-frequency asymptote. (8)}$$

The velocity  $v_o$  remains constant until inertial effects gain relevance at high frequencies, when the excitation frequency approaches  $\omega_{\text{rel}} \approx \psi/m$ , which in this case becomes,

$$\omega_{\text{rel}} \approx \frac{\sqrt{n_+ \psi_+ n_- \psi_-}}{M_s} \quad \text{transition frequency. (9)}$$

The transition frequency in electrolytes and soil systems is several orders of magnitude greater than the frequency of interest in this study. Figure 5 shows the electrical mechanical energy coupling response in a 0.5 M NaCl electrolyte predicted with this model.

In the case of dipolar molecules, the application of an electric field causes orientational polarization (Santamarina *et al.*, 2001). If the center of rotation is not concentric with the center of mass, a macro-scale mechanical response will take place.

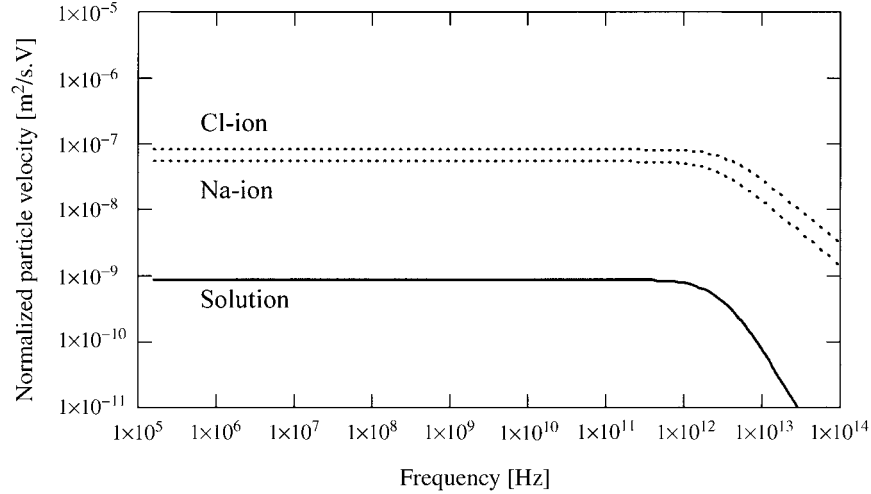


Figure 5. Predicted electrical-mechanical energy coupling response in a 0.5 M NaCl electrolyte. Normalized response versus frequency. The velocity of individual ions and the solution are shown.

### 3.3. COMMENTS

The following observations follow from the previous analyses of the mechanical-electrical and electrical-mechanical dynamic couplings.

- Dynamic coupling effects are more evident in systems where the charged elements have high contrast in  $m \cdot z/r$ , where the mass  $m$  captures inertia effects, the charge  $z \cdot e_0$  relates to electric effects and the size  $r$  is relevant for the viscous drag.
- The input signal and the response are of the same frequency in both effects. Yet, there is a frequency dependent phase shift (see Equation (5) – a similar time-varying response can be written for electrical-mechanical coupling).
- Each phenomenon has a transition frequency that separates the range where viscous and inertial forces control the response of the system. At frequencies below the transition frequency viscous forces control the behavior. At frequencies above the transition frequency inertial effects become dominant, and the system response drops.

## 4. Identification of Coupling Mechanisms in Suspensions and Soils

The previous section highlighted the fundamental mechanisms for dynamic energy coupling in media with charged components; the case of electrolytes is particularly relevant and was used to demonstrate the effect. In this section, the discussion is extended to the case of mineral suspensions and soils.

### 4.1. DYNAMIC ENERGY COUPLING IN SUSPENSIONS

When a suspension of fine mineral particles is mechanically excited, the differential inertia between the fluid and the mineral results in the displacement of particles relative to the fluid. Slip occurs along the shear plane, and an electrical dipole forms between the particle and the displaced counter ion cloud (Figure 2(d)). Conversely, the application of an electric field causes the displacement of the particles and its ion cloud in opposite directions. Conservation of momentum explains the mechanical excitation observed at the macro-scale. Hence, the time varying electric field triggers an oscillatory motion in charged particles and ions (Lyklema, 1995; Rasmusson *et al.*, 1997).

Double layer phenomena are critical in both mechanisms. Double layer effects are important in high specific surface minerals and when the pore fluid has low conductivity. As the conductivity of the pore fluid increases, double layers become thinner, the zeta-potential on the shear plane decreases, ions in the bulk fluid readily diffuse in-and-out of the counter ion cloud preventing polarization, electrical conduction is determined by the hydrated ions in the bulk electrolyte, and the contribution of double layer polarization to coupled energy phenomena decreases.

The dynamic mobility of charged particles  $u$  [ $\text{m}^2\text{s}^{-1}\text{V}^{-1}$ ] is the electrophoretic mobility of particles under the action of a time-varying electric field. Expressions similar to those derived above (Equations (5) and (8)) can be obtained for both the mechanical- electrical and the electro-mechanical coupling in terms of dynamic mobility of particles  $u$ . However, there are three components in electrolytes (hydrated cations, hydrated anions, and free water molecules), while there are only two components in suspensions: charged particles and the fluid (which in this case includes the counterions). The resulting equations are of the following form (O'Brien, 1988; Goetz and El-Aasser, 1992; Lyklema, 1995, Equations 4.3.43 and 4.3.44):

$$\phi = \left[ (1 - n)u \frac{\Delta\rho}{\rho} \frac{v_s V}{\sigma} \right] F \quad \text{mechanical-electrical coupling,} \quad (10)$$

$$v_o = [(1 - n)u \Delta\rho E] F' \quad \text{electrical-mechanical coupling,} \quad (11)$$

where  $\phi$  is the potential,  $1 - n$  is the volume fraction of particles in the solution,  $\Delta\rho$  is the density difference between the mineral and the fluid phase [ $\text{kg}/\text{m}^3$ ],  $\rho$  is the density of the suspension [ $\text{kg}/\text{m}^3$ ],  $V$  is the velocity of P-waves in the suspension,  $v_o$  is the particle velocity of the suspension,  $\sigma$  is the effective conductivity of the dispersion (frequency dependent). The dimensional coefficients  $F$  [ $\text{kg}/\text{m}^3$ ] and  $F'$  [ $\text{m}^3/\text{kg}$ ] are geometric factors that depend on the experimental device (Goetz and El-Aasser, 1992).

The charge assigned to the particle is computed from the zeta potential  $\zeta$  [V] (Figure 1). Then, the low frequency approximation to the dynamic mobility  $u$  is

$$u = \frac{\kappa_s \varepsilon_o \zeta}{\eta} \quad \text{low-frequency asymptote.} \quad (12)$$

This relation applies for non-interacting particles and when the particle diameter to double layer thickness ratio is high. The main relaxation is

$$\omega_r = \frac{\eta}{r^2 \rho} \quad \text{transition frequencys.} \quad (13)$$

The complete formulation and further details can be found in O'Brien (1988), Loewenberg and O'Brien (1992), and Lyklema (1995). Figure 6 presents the dynamic mobility predicted with this model. The large relaxation observed in the figure is controlled by the ratio between inertial and viscous forces. The response also shows a small relaxation at low frequencies, which relates to the ratio between the permittivity and the conductivity of the medium.

#### 4.2. DYNAMIC ENERGY COUPLING IN SOILS

Particles in soils form a skeleton with shear stiffness. As the frequency of propagating fast P-wave and S-wave increases, inertial effects increase with  $\omega^2$ , while

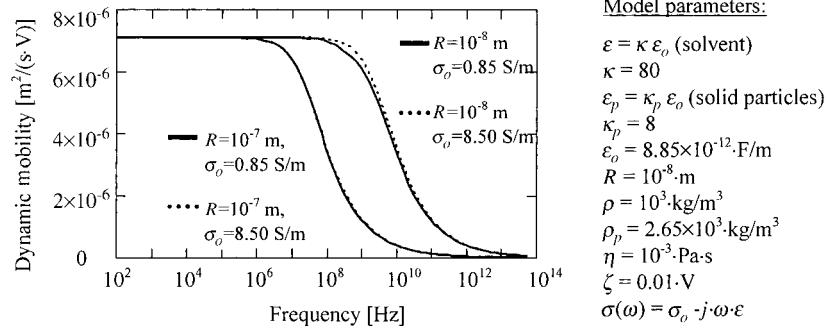


Figure 6. Dynamic energy coupling of suspension of spherical particles as modeled by Loewenberg and O'Brien (1992). Results for the dynamic mobility of particulate with same radius  $R$ , but for electrolytes with different DC conductivity, superimpose.

viscous shear between the fluid and the pore walls increases with,  $\omega$ ; thus, the fluid tends to remain in place, moving relative to the skeleton at frequencies near Biot's characteristic frequency

$$f_c = \frac{n\eta}{2\pi\rho_f K} = \frac{ng}{2\pi k}, \quad (14)$$

where  $n$  is the porosity of the soil [],  $\eta$  is the viscosity of the fluid (for water at room temperature  $\eta = 10^{-3}$  Pa·s),  $K$  [ $\text{m}^2$ ] is the absolute hydraulic permeability of the porous medium,  $k$  [m/s] is the hydraulic conductivity for water,  $\rho_f$  [ $\text{kg}/\text{m}^3$ ] is the mass density of the fluid, and  $g = 9.81$   $\text{m}/\text{s}^2$  is gravity.

Biot's slow P-wave (Biot 1956a, b) is a diffusional propagation and produces the relative displacement of the fluid with respect to the soil matrix even at low frequencies. Shear along pore walls displaces charges in the counterion cloud and a streaming electrical potential develops. Mode conversion at interfaces between poroelastic media convert incident  $P$  or  $SV$  propagation into slow-P, fast-P, and  $SV$  reflections and refractions. Therefore, interfaces promote mechanical-electrical coupling (see Thompson and Gist, 1993; Butler *et al.*, 1996; Mikhailov *et al.*, 1997; Zhu and Toksoz, 1997). Because the slow P-wave attenuates rapidly (e.g. the damping ratio can be 200%), only a small volume of the formation near the source or near interfaces contributes to the generation of the electromagnetic response. The mechanical-electrical coupling is often known as 'seismo-electric effect.' This effect can also take place in saturated jointed rock masses and in unsaturated soils.

In an attempt to model dynamic energy coupling effects in porous media, Neev and Yeatts (1989) added electric forces in terms of streaming potentials and electro-osmotic pressure to Biot's equations of motion. Their solution shows the presence of three characteristic frequencies. These frequencies involve the viscous-inertial forces, the frequency-dependent conductivity, and the zeta potential. A more comprehensive formulation is presented in the work by Pride and co-workers who

combine Biot's equations with Maxwell's equations (Pride and Morgan 1991; Pride 1994; Pride and Haartsen, 1996).

The electrical-mechanical energy coupling in soils is known as 'electro-seismic effect.' It can be explained by taking into consideration the acceleration of charges in the electrolyte and in the counterion cloud outside the shear plane, while conserving the momentum of the whole skeleton-fluid system. The displacement of charges is limited within the soil skeleton by the presence of transverse boundaries, that is, pore walls. Therefore, spatial, Maxwell-Wagner interfacial polarization is involved in this coupling (polarization mechanisms are described in Santamarina *et al.*, 2001). The total coupling of mechanical and electrical energy in suspensions and soils includes the response of the pore fluid itself as discussed previously in the context of electrolyte.

### 5. Important Inconsistencies in Published Experimental Studies

Laboratory and field studies are summarized in Tables II and III. The following observations can be made.

- Laboratory studies have been conducted at high frequencies (with electrodes spaced at  $\lambda/2$ ), while field studies have been conducted at low frequencies.
- *Electrical-mechanical coupling (Table II)*. There are limited experimental studies. Out of the three studies found in the literature, only one high frequency laboratory study documents the coupling coefficient; the measured value is about one order of magnitude higher than the response obtained with theoretical models (refer to Figure 5).
- *Mechanical-electrical coupling (Table III)*. High-frequency laboratory data agrees with theoretical predictions. However, coupling values obtained in field studies are several orders of magnitude higher than expected on the bases of coupling mechanisms identified earlier.
- Further analysis of the mechanical-electrical data obtained by Long and Rivers (1975) shows that the mechanical-electrical response correlates best with wave propagation components that have particle motion normal to the electrode (P and Rayleigh waves), and it has virtually no correlation with transverse wave components.

The discrepancy between theory and low-frequency field studies is surprising, particularly in view of the apparent agreement between theoretical predictions and high frequency laboratory data.

### 6. New Laboratory Experimental Study at Low Frequency

The laboratory experimental study described herein was specifically designed to explore the significant differences between high-frequency laboratory studies and low-frequency field observations identified above, by implementing low-frequency

Table II. Electrical-mechanical effect – conflicting laboratory and field evidence

Reference	Test	Frequency	Soil/water system	Setup	Measured magnitude
Zhu <i>et al.</i> (1994)	Laboratory tests.	400 V pulse excitation.	Water saturated Berea sandstone. Cylindrical specimen.	Electrodes wrapped along the length of the specimen.	Authors observed a response. The magnitude is not documented.
Rasmusson <i>et al.</i> (1997)	Laboratory tests.	0.5–11 MHz	Sodium bentonite solutions (volume fraction: 0.008, pH 10.2, background solution 2.5–18 mM NaCl).	AcoustoSizer (dynamic mobility instrument).	Normalized response: $2.25$ to $3.05 \times 10^{-8}$ $\text{m}^2/(\text{V}\cdot\text{s})$ . The response decreases with frequency.
Thompson and Gist (1993)	Field tests.	150 A pulse signal.	Saturated sand and shale formations.	Electric source: 300 m separated electrodes. Receivers: hydrophones in cased boreholes.	Authors observed a response. The magnitude is not documented.

Table III. Mechanical-electrical effect – conflicting laboratory and field evidence

Reference	Test	Frequency	Soil/water system	Setup	Measured magnitude
Zana and Yeager (1982)	Laboratory tests	>200 kHz	Electrolyte solutions	Harmonic source. Thin Pt wire probes. Measurements at $\lambda/2$ .	NaCl solutions at 22°C: $1 \times 10^{-4}$ V·s/m (0.003 mol/l) $7 \times 10^{-5}$ V·s/m (0.03 mol/l) $6 \times 10^{-5}$ (0.03 mol/l).
					CsCl solutions at 22°C: $1 \times 10^{-4}$ V·s/m (0.003 mol/l) $7 \times 10^{-5}$ V·s/m (0.03 mol/l) $6 \times 10^{-5}$ V·s/m (0.3 mol/l).
Zhu <i>et al.</i> (1994)	Laboratory tests	~40 kHz (P-waves) $\lambda \sim 0.1$ m	Water saturated porous Berea and Cocinino sandstone. Cylindrical specimens.	Waveguide specimen. One contact electrode with respect to ground.	Observed: 80 to $200 \times 10^{-6}$ V. Particle velocity: not presented. Response is particle velocity dependent.
		~50 kHz (Surface-waves)	Water saturated Berea sandstone.	P-wave & contact electrodes.	Observed: $50 \times 10^{-6}$ V Particle velocity:

Table III. (continued).

Reference	Test	Frequency	Soil/water system	Setup	Measured magnitude
		$\lambda \sim 0.05$ m	Plate-like specimen.	One contact electrode with respect to ground.	not presented. Response is particle velocity dependent.
Long and Rivers (1975)	Field tests	$\sim 15$ Hz	Coastal plain sedimentary rocks.	Explosive source and Wenner array.	Observed: $> 10^{-1}$ V·s/m
Thompson and Gist (1993)	Field tests	30–40 Hz	Saturated sand and shale. Dipole antennas: 12 m long formations.	Explosive source Location: 80 m Electrical response $\sim 110$ Hz	Measured: $0.7 \times 10^{-7}$ V from source Estimated <sup>a</sup> : $\sim 10^{-3}$ V·s/m
Butler <i>et al.</i> (1996)	Field tests	70–100 Hz	Interface between organic-rich fill and impermeable glacial till.	Sledgehammer and explosive sources. Surface and borehole electrodes.	Measured: $2.5 \times 10^{-3}$ V Location: $\sim 3$ m from Interface Estimated <sup>a</sup> : $\sim 2.5$ V·s/m



Table III. (continued).

Reference	Test	Frequency	Soil/water system	Setup	Measured magnitude
Mikhailov <i>et al.</i> (1997)	Field tests	60–150 Hz	Interface between unsaturated and saturated glacial till.	Sledgehammer and explosive sources Dipole antennas (porous pot Ag-AgCl electrodes)	Measured: $\sim 0.8 \times 10^{-3}$ V Location: $\sim 3$ m from interface Estimated <sup>a</sup> : $\sim 0.8$ V·s/m

<sup>a</sup>Note: Estimated normalized values are based on the measured electrical response (voltage) and estimated particle velocities based on the characteristics of the source, site conditions and the distance.

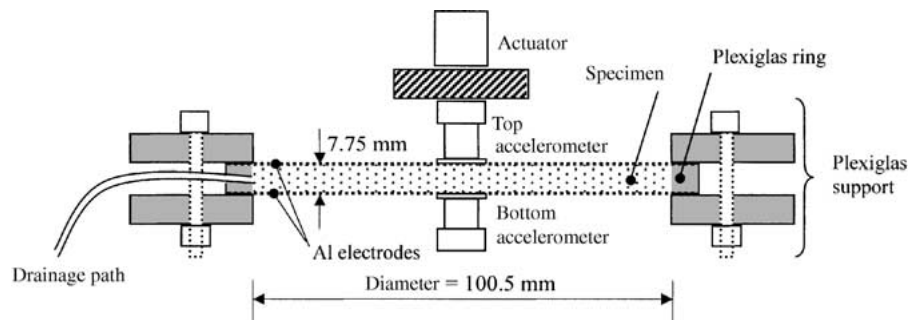


Figure 7. Device used to monitor mechanical-electrical and electrical-mechanical coupling phenomena in soils. The actuator is detached during electrical-mechanical coupling tests.

field conditions in the laboratory. The description of the cell designed for this study, and results obtained with various electrolytes and soils at different confinement and saturation are summarized next. Both, the mechanical-electrical and electrical-mechanical couplings are explored.

#### 6.1. EXPERIMENTAL DEVICE

Low-frequency energy couplings are explored with the device shown in Figure 7. The specimen is placed inside a Plexiglas ring (100.5 mm inside diameter and 7.8 mm height) and is bound by two aluminum foil sheets. The aluminum foil sheets not only act as flexible supporting membranes for the specimen but they also act as electrodes during testing. A piezoelectric actuator (AVC Model 712A01 piezoelectric actuator) generates the mechanical excitation. Two Columbia 8402 accelerometers (sensitivity: 100 mV/g) are used to monitor the vibration in the specimen. The setup is placed inside a chamber, and the specimen is confined by pressurizing the chamber. The increase in confinement increases the specimen stiffness and secures the contact between the electrodes and the specimen.

The electrical response in the mechanical-electrical effect is filtered and amplified (Krohn-Hite Model 3944) and fed to a Stanford Research SR 795 Signal Analyzer. The filter-amplifier is set to 20 kHz low-pass and 20-dB gain. The signal generator in the analyzer is used to feed a sinusoidal frequency sweep to the mechanical actuator during mechanical-electrical coupling testing, and to the electrodes during the electrical-mechanical coupling monitoring. The signal analyzer also allows computing the power spectra and the frequency response between input and output channels. Signal stacking is used in this study to further improve the signal-to-noise ratio (up to 128 events).

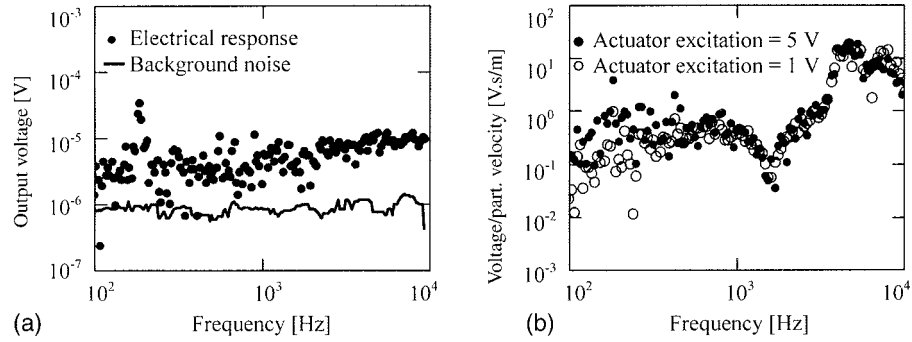


Figure 8. Mechanical-electrical coupling phenomena in 0.5 M NaCl electrolyte specimens. The response is higher than the measured background noise. The input particle velocity is not constant.

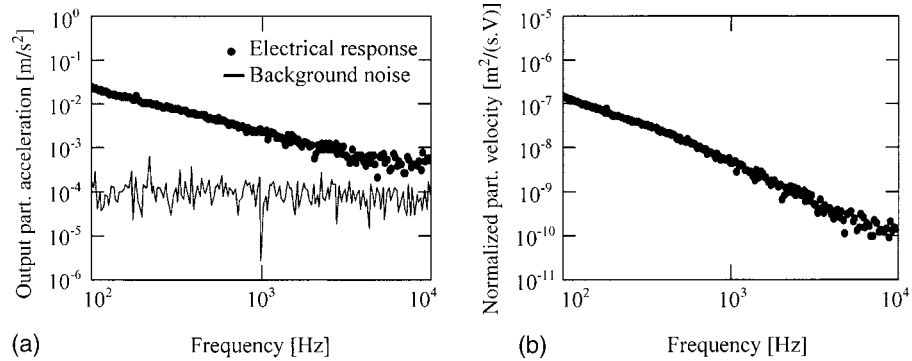


Figure 9. Electrical-mechanical coupling phenomena in 0.5 M NaCl electrolyte specimens. The response is higher than the measured background noise.

## 6.2. LOW FREQUENCY ENERGY COUPLING IN ELECTROLYTES

Figures 8 and 9 present experimental results for the low-frequency mechanical-electrical and electrical-mechanical energy coupling response in a 0.5 M NaCl electrolyte. The following observations can be made.

- The background noise is plotted in Figures 8(a) and 9(a); the response amplitude is significantly higher than the noise level.
- Figures 9(b) and 10(b) show the output normalized by the input for (Note: the input in the mechanical-electrical coupling is the velocity determined with the accelerometers).
- Results are shown for two excitation levels in Figures 8(b) and 9(b). In both coupling effects, the normalized response appears superimposed, suggesting that coupling in this study is a linear effect. (Note that the mechanical properties of the test setup and driving systems are evidenced in spectral peaks.)

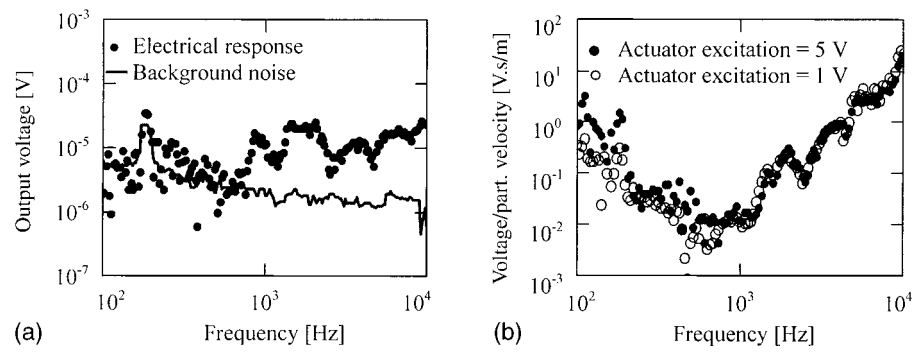


Figure 10. Mechanical-electrical coupling phenomena in a kaolinite specimen under 25 kPa confinement. The response is higher than the measured background noise for frequencies higher than 800 Hz.

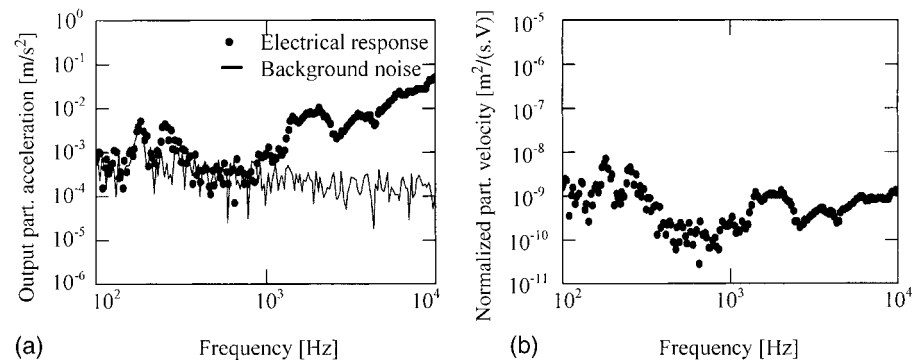


Figure 11. Electrical-mechanical coupling phenomena in a kaolinite specimen under 25 kPa confinement. The response is higher than the measured background noise for frequencies  $f$  higher than 800 Hz.

- The normalized mechanical-electrical response variation with frequency in both coupling effects differs from the frequency-independent response predicted in models for this frequency range.
- The measured mechanical-electrical response is about three orders of magnitude larger than the predicted response (compare Figure 4 and Figures 8(a) and 8(b)). This is analogous to the low-frequency field measurements summarized in Table III.

### 6.3. LOW FREQUENCY ENERGY COUPLING EVIDENCE IN KAOLINITE

A soft kaolinite specimen (gravimetric water content  $w\% = 25$ ) is tested in the same device shown in Figure 7. The specimen is subjected to 25 kPa confining pressure. The results are presented in Figures 10 and 11. Figures 10(a) and 11(a) show the response and the background noise. The system response increases above

the background noise at about 800 Hz, in both mechanical-electrical and electrical-mechanical test results.

The normalized response for both coupling effects is presented in Figures 10(b) and 11(b). Two input excitation levels is shown in Figure 10(b). Once again, the superposition of the two trends suggests linear coupling mechanisms. Other observations made for electrolytes apply to this kaolinite specimen as well.

The particle velocity that develops in the specimen reflects the mechanical properties of the test setup. This is particularly important in the electrical-mechanical response, where normalization is done against a constant input voltage. Similar tests for both coupling effects were performed at various confining pressures and rendered similar order-of-magnitude response and frequency-dependent variation. Further details are presented next.

## 7. Plausible Hypotheses

The match between theory-based predictions and high frequency laboratory measurements, the similarity between the new low frequency laboratory measurements gathered in this study and previously published low frequency field measurements, and the disparity between low frequency and high frequency measurements suggest common underlying trends related to frequency effects. The following hypotheses are suggested to account for the differences.

- Noise and experimental difficulties.
- System dynamics.
- Wavelength to electrode spacing ratio (mechanical-electrical coupling).
- Electrode effects.

The development of unsuspected low frequency polarization/conduction mechanisms should not be discarded. Yet, no mechanism besides those discussed in the review is envisioned at this point. Hence, emphasis is placed on measurement effects.

### 7.1. NOISE AND EXPERIMENTAL DIFFICULTIES

The response sought is a low amplitude signal. The poor signal-to-noise ratio observed in experimental studies confirms the weak nature of these coupling phenomena in comparison with cultural noise. Improper shielding, pseudo-piezoelectric effect in glass cells, streaming potentials, condenser effect between the electrodes and their housing and the vibration of faulty connections can alter measurements and add noise.

Several published studies document methodologies used to improve the strength of the signals during testing (see Zana and Yeager, 1982; Butler and Russell, 1993). Noise control involves mechanical isolation (critical in electrical-mechanical

coupling studies) and shielding-grounding (critical in mechanical-electrical coupling studies – see guidelines in Wright, 1995). Signal stacking is an effective procedure to cancel no-coherent noise thus increasing the signal-to-noise ratio. However, some sources of noise may cause signals in phase with the signatures under study. Examples include plastics such as Plexiglas that become charged during assembly, and faulty-connections. These sources must be identified and removed by proper experimental design.

### 7.2. WAVELENGTH-TO-ELECTRODE SPACING RATIO (MECHANICAL-ELECTRICAL COUPLING)

The maximum mechanical-electrical potential predicted with Equation (5) is measured with two electrodes  $\lambda/2$  apart, as indicated in Figure 3. This is not the case in low frequency measurements conducted in the field or in our laboratory specimens. In the absence of boundary or electrode effects, the voltage measured at frequency  $\omega$  between two electrodes at distance  $L$  is related to the maximum potential  $\phi$  measured at  $\lambda/2$  as

$$\frac{\Delta V}{\phi} = \pi \frac{L}{\lambda} = \frac{L\omega}{2V}, \quad (15)$$

where  $V$  is the velocity of the propagating mechanical wave.

### 7.3. ELECTRODE EFFECTS: ‘ELECTROMAGNETIC FREQUENCY RESPONSE OF THE CELL’

Monitoring the mechanical-electrical coupling involves an electrical circuit where the soil specimen is in series with electrodes and the required peripheral electronics. Therefore, the soil-electrode interface sees the movement of ions on the soil side, and the movement of electrons on the electronics side. Electrodes that do not experience oxidation-reduction are called blocking electrodes (e.g. platinum; within the frequency range of seismic events of interest, all metal electrodes effectively perform as blocking electrodes). When blocking electrodes are used, ions accumulate at the interface causing electrode polarization.

This situation can be modeled by adding a thin air-gap  $d_{\text{gap}}$  [m] at the interface between the electrode and the soil. Consider a parallel plate capacitor with a soil specimen of thickness  $d_s$  [m] (Figure 12 (a)). The soil can be represented as a resistor and a capacitor in parallel, with effective electric conductivity  $\sigma_s$  [mohs/m] and dielectric permittivity  $\varepsilon_s$  [F/m]. Then, the complete circuit for the measurement is

$$\begin{aligned} V_{\text{meas}} = IZ_{\text{eq}} &= I \left( \frac{1}{j\omega C_{\text{gap}}} + \frac{1}{(1/R_s) + j\omega C_s} \right) \\ &= \frac{I}{A} \left[ \frac{d_{\text{gap}}}{j\omega \varepsilon_o} + \frac{d_s}{\sigma_s + j\omega \varepsilon_s} \right], \end{aligned} \quad (16)$$

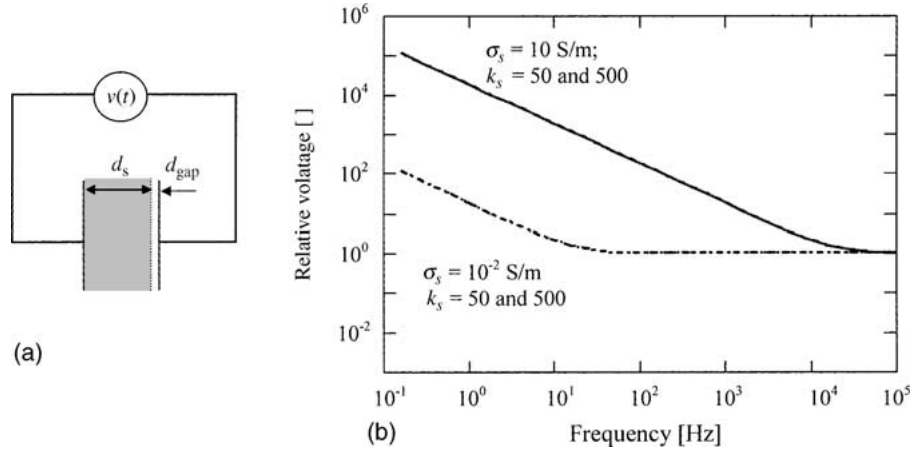


Figure 12. Electrode polarization effects in low frequency measurements of energy coupling.

where  $I$  [A] is the electrical current,  $Z_{eq}$  [ $\Omega$ ] is the equivalent impedance of the system,  $C_{gap}$  [F] is the capacitance of the gap,  $R_s$  [ $\Omega$ ] and  $C_s$  [F] are the resistance and capacitance of the specimen, and  $A$  is the cross sectional area of the capacitor. The measured potential  $V_{meas}$  [V] depends on the frequency of the mechanical excitation  $\omega$ , and can be related to the true potential that develops within the soil mass  $\phi$  as follows.

$$\frac{V_{meas}}{\phi} = \frac{(d_{gap}/j\omega\epsilon_0) + (d_s/(\sigma_s + j\omega\epsilon_s))}{(d_s/(\sigma_s + j\omega\epsilon_s))} \approx 1 + \frac{\sigma_s}{j\omega\epsilon_0} \frac{d_{gap}}{d_s}. \quad (17)$$

In field applications, the value  $d_s$  is in the order of the electrode diameter. The effective value of  $d_{gap}$  may vary from few angstroms in smooth clean electrodes, to several nanometers in rough or altered electrodes (Klein and Santamarina, 1997).

Figure 12(b) shows the variation of the measured potential  $V_{meas}$  as a function of frequency for a range in soil parameters  $\sigma_s$  and  $\kappa_s$  that covers common situations (Note: the conductivity and permittivity of the electrolyte or soil specimen are assumed constant in this analysis. This is not the case in real specimens: as frequency decreases, the effective conductivity decreases reaching  $\sigma_{DC}$ , while the permittivity increases. The selected range of parameters in Figure 12(b) can accommodate this variation). Equation (16) and these results show that the higher the conductivity of the specimen  $\sigma_s$ , the lower the frequency and the wider the gap, then, the higher the charge accumulation at electrodes, and the higher the measured potential  $V_{meas}$ . In general, electrode polarization ceases to affect the measured potential at frequencies higher than 20–100 kHz. Therefore, electrode polarization effects are not expected in high-frequency laboratory measurements. On the other hand, electrode polarization effects may cause differences in three orders of magnitude at  $f \sim 1$  kHz.

The electrical-mechanical coupling is also affected by electrode effects. In this case, the applied field is partially shielded by the accumulation of charge at the

electrodes, and the effective potential  $V_{\text{eff}}$  felt by the specimen is related to the applied potential  $V_{\text{app}}$  as

$$\frac{V_{\text{eff}}}{V_{\text{app}}} = \frac{(d_s/(\sigma_s + j\omega\varepsilon_s))}{(d_{\text{gap}}/j\omega\varepsilon_o) + (d_s/(\sigma_s + j\omega\varepsilon_s))}. \quad (18)$$

This relation is the inverse of Equation (17), and it predicts that the lower frequency, the lower the potential that is effectively applied to the soil. Hence, the resulting mechanical vibration should be smaller at lower frequencies, contrary to the response observed in Figure 9(b).

#### 7.4. SYSTEM DYNAMICS: ‘MECHANICAL FREQUENCY RESPONSE OF THE CELL’

The mechanical-electrical response is normalized with respect to the input velocity, therefore, the inherent dynamic response of the system is taken into consideration. This is not the case in the electrical-mechanical response, where the normalization is done with respect to the input voltage. Thus, the mechanical frequency response of the cell affects the measured coupling. The low frequency resonant mode is the membrane-type resonance of the specimen. Higher-frequency resonant peaks develop when the P-wave wavelength approaches two times the specimen thickness,  $\lambda=2\cdot L$ . Resonance amplifies particle motion. (Note that the electromagnetic wavelength is orders of magnitude longer than laboratory specimen in the Hz-kHz region, and the specimen can be considered as a lump-parameter circuit system).

Therefore, the system dynamic response acts as a low pass frequency-dependent filter of the true material response. This may explain, at least in part, the  $-2:1$  response in log-log scale observed in Figures 10 and 12. The electrical-mechanical response gathered in kaolin specimens confined at 25, 50, and 200 kPa show that spectral peaks shift to lower frequencies and increase in amplitude as the confining pressure increases.

## 8. Conclusions

The phenomena of mechanical-electrical and electrical-mechanical coupling can be explained through simple micro-scale conceptual models that include electrical, inertial, and viscous forces, continuity and conservation of momentum. These conceptual models permit the interpretation of energy coupling phenomena in electrolytes, suspensions, and porous media.

Energy coupling phenomena in porous media are governed by the relative displacement of the fluid solid-matrix primarily in the Biot’s slow P-wave regime. Therefore, coupling concentrates at the boundaries where mode conversions occur.

Coupling coefficients predicted with theoretical models are similar to those measured in the laboratory in high-frequency studies. However, there is a very significant mismatch between those values and the coupling coefficients observed



in low frequency field studies. The low frequency measurements implemented in this study to simulate field measurements rendered results comparable to those observed in field studies.

Experimental design plays a critical role in the study and monitoring of coupling effects in the lower frequencies relevant to field applications ( $f < 10$  kHz). The 'mechanical frequency response' of the cell appears to play a critical role in the electrical-mechanical response that is observed. Electrode effects in the 'electromagnetic frequency response' of the cell affects the results in the two coupling effects, increasing the observed mechanical-electrical coupling and decreasing the observed electrical-mechanical response. While electrode effects cannot explain the spectral variation in either case, it is clear that electrode effects control the assessment of dynamic mechanical and electrical energy coupling in the frequency of interest to potential engineering applications (less than  $\sim 10^4$  kHz). In this frequency range, the material response is below the viscous-inertial transition frequencies.

The particle motion (input in mechanical-electrical coupling or output in electrical-mechanical coupling) varies with the working frequency in relation to the resonant modes of vibration in the system or the testing device. Furthermore, the relative separation of the electrodes with respect to the wavelength, renders an observed potential that increases with frequency.

Evidence of electrical-mechanical and mechanical electrical energy coupling phenomena is presented for both electrolytes and saturated kaolinite systems. Tests show variation of the response with frequency and with the stiffness of the specimens. The response appears linear with the amplitude of the input, within the tested range.

### Acknowledgement

This research is supported by grants from the National Science Foundation. Mathematic files with the models presented in this paper are available from the authors.

### References

- Belluigi, A.: 1937, Seismo-electric prospecting, *Oil Weekly* **87** (November 29), 38–42.
- Biot, M. A.: 1956a, Theory of propagation of elastic waves in a fluid-saturated porous solid. I. Low-frequency range, *J. Acoust. Soc. Amer.* **28**(2), 168–178.
- Biot, M. A.: 1956b, Theory of propagation of elastic waves in a fluid-saturated porous solid. II. High-frequency range, *J. Acoust. Soc. Amer.* **28**(2), 179–191.
- Bourbié, T., Coussy, O. and Zinszner, B.: 1987, *Acoustic of Porous Media*, Gulf Publishing Company, Houston, TX, 325 pp.
- Butler, K. E., Russell, R. D., Kopic, A. W. and Maxwell, M.: 1996, Measurements of the seismoelectric response from a shallow boundary, *Geophysics* **61**(6), 1769–1778.
- Debye, P.: 1933, A method for the determination of the mass of electrolytic ions, *J. Chem. Phys.* **1**, 13–17.
- Goetz, R. J. and El-Aasser, M. S.: 1992, Effects of dispersion concentration on the electroacoustic potentials of o/w miniemulsions, *J. Colloid. Interface Sci.* **150**(2), 436–452.

- Hermans, J. J.: 1938, Charged colloid particles in an ultrasonic field, *London, Edinburg, Dublin Phil. Mag.* **25**, 426–438.
- Holden, A.: 1965, *The Nature of Solids*, Dover Publications, New York, 241 pp.
- Ikeda, T.: 1990, *Fundamentals of Piezoelectricity*, Oxford Univ. Press, Oxford, 263 pp.
- Israelachvili, J.: 1992, *Intermolecular and Surface Forces*, 2nd edn., Academic Press, London, 460 pp.
- Klein, K. and Santamarina, J. C.: 1997, Broad-band frequency measurements with electromagnetic waves, *ASTM Geotech. Test. J.* **20**(2), 168–178.
- Long, L. T. and Rivers, W. K.: 1975, Field measurements of the electroseismic response, *Geophysics* **40**, 233–245.
- Loewenberg, M. and O'Brien, R. W.: 1992, The dynamic mobility of non-spherical particles, *J. Colloid. Interface Sci.* **150**(1), 148–168.
- Lyklema, J.: 1995, *Fundamentals of Interface and Colloid Science*, Vol. II: *Solid and Liquid Interfaces*, Academic Press, London.
- Martner, S. T. and Sparks, N. R.: 1958, The electroseismic effect, *Geophysics* **24**, 297–308.
- Mikhailov, O. V., Haartsen, M. W. and Toksöz, M. N.: 1997, Electroseismic investigation of the shallow subsurface: field measurements and numerical modeling, *Geophysics* **62**(1), 97–105.
- Mitchell, J. K.: 1991, Conduction phenomena: from theory to geotechnical practice, The 31st Rankine lecture, *Geotechnique* **41**, 299–340.
- Neev, J. and Yeatts, F. R.: 1989, Electrokinetic effects in fluid-saturated poroelastic media, *Phys. Rev. B.* **40**(1), 9135–9141.
- O'Brien, R. W.: 1988, Electro-acoustic effects in a dilute suspension of spherical particles, *J. Fluid Mech.* **190**, 71–86.
- Pride, S. R. and Morgan, F. D.: 1991, Electrokinetic dissipation induced by seismic waves, *Geophysics* **56**(7), 914–925.
- Pride, S. R.: 1994, Governing equations for the coupled electromagnetic and acoustic of porous media, *Phys. Rev. B.* **15**, 15678–15696.
- Pride, S. R. and Haartsen, M. W.: 1996, Electroseismic wave properties, *J. Acoust. Soc. Amer.* **100**, 1301–1315.
- Rasmusson, M., Rowlands, W., O'Brien, R. W. and Hunter, R. J.: 1997, The dynamic mobility and dielectric response of sodium bentonite, *J. Colloid Interface Sci.* **189**, 92–100.
- Santamarina, J. C., Klein, K. A. and Fam, M. A.: 2001, *Soils and Waves*, Wiley, Chichester, 488 pp.
- Stoll, R. D.: 1977, Acoustic waves on ocean sediments, *Geophysics* **42**, 715–725.
- Thompson, A. H. and Gist, G. A.: 1993, Geophysical applications of electrokinetic conversion, *Leading Edge* (December 1993), 1169–117.
- Thompson, R.: 1936, The seismic electric effect, *Geophysics* **1**, 327–335.
- White, J. E.: 1983, *Underground Sound. Application of Seismic Waves*, Elsevier, Amsterdam, 253 pp.
- Wright, C. P.: 1995, *Applied Measurement Engineering: How to Design Effective Mechanical Measurement Systems*, Prentice-Hall, Englewood Cliffs, NJ, 402 pp.
- Zana, R. and Yeager, E. B.: 1982, Ultrasonic vibration potential, In: J. Bockris, B. Conway and R. White (eds), *Modern Aspects of Electrochemistry*, No. 14, Plenum Press, New York and London, pp. 1–60.
- Zhu, Z., Cheng, C. H. and Toksoz, M. N.: 1994, Electrokinetic conversion in fluid saturated rock porous sample, Expanded Abstract, *64th SEG International Conference*, Dallas, 1997, pp. 1057–1060.
- Zhu, Z. and Toksoz, M. N.: 1997, Experimental studies of electrokinetic conversion in fluid saturated borehole models, Expanded Abstract, *67th SEG International Conference*, Dallas, 1997, pp. 334–337.